Tracking Endocardial Motion Via Multiple Model Filtering

Kumaradevan Punithakumar*, Ismail Ben Ayed, Ali Islam, Ian G. Ross, and Shuo Li

***Abstract*—Tracking heart motion plays an essential role in the diagnosis of cardiovascular diseases. As such, accurate characterization of dynamic behavior of the left ventricle (LV) is essential in order to enhance the performance of motion estimation. However, a single Markovian model is not sufficient due to the substantial variability in typical heart motion. Moreover, dynamics of an abnormal heart could be very different from that of a normal heart. This study introduces a tracking approach based on multiple models, each matched to a different phase of the LV motion. First, the algorithm adopts a graph cut distribution matching method to tackle the problem of segmenting LV cavity from cardiac MR images, which is acknowledged as a difficult problem because of low contrast and photometric similarities between the heart wall and papillary muscles within the LV cavity. Second, interacting multiple model (IMM), an effective estimation algorithm for Markovian switching system, is devised subsequent to the segmentations to yield state estimates of the endocardial boundary points. The IMM also yields the model probability indicating the model that most closely matches the LV motion. The proposed method is evaluated quantitatively by comparison with independent manual segmentations over 2280 images acquired from 20 subjects, which demonstrated competitive results in comparisons with related recent methods.**

***Index Terms*—Cardiac wall motion estimation, interacting multiple model (IMM) algorithm, MRI, Markovian switching systems, recursive Bayesian filtering.**

I. Introduction

EARLY detection of heart wall motion abnormality is of utmost importance in the diagnosis and control of coronary heart disease. As such, tracking and quantitative scoring of heart motion is of capital importance in clinical use. MR sequences are widely used for analyzing cardiac function, and provide a large number of images.[1] Therefore, tracking based on manual delineation of the left ventricular (LV) boundary in all these images is prohibitively time-consuming, and automating the process has been the subject of an intense research effort recently [1]–[6].

Segmenting LV cavity from MR images is very difficult due to the low contrast and photometric similarities between connected cardiac regions, for instance, the papillary muscles within the cavity and heart wall have approximately the same intensity. Therefore, standard segmentation methods based solely on intensity information cannot yield accurate tracking. To overcome this difficulty, most of existing methods constrain the solution with prior geometric properties, such as the shape of the LV cavity learned *a priori* from a finite-training set [7]–[9]. Unfortunately, such training information is not sufficiently reliable to recover the substantial variability between subjects [10]. First, to tackle the problem of segmenting LV cavity, this study adopts the graph cut distribution matching (GCDM) [11], which yields initial segmentation of the LV cavity within each frame by keeping the same photometric/geometric distribution of the cavity over cardiac cycles. This is done by minimizing a distribution-matching energy, which measures the similarity between a given segmentation of the first frame and the unknown segmentation of the current frame. Based on global distribution information learned from the first frame in the current data, GCDM overcomes some of the difficulties inherent to cardiac images without resorting to *a priori* training.

Subsequently, a multiple model approach is devised to constrain the segmentation results with prior knowledge of temporal consistency. Incorporation of such prior knowledge, which characterizes the dynamic behavior of the LV motion, enhances the accuracy of both segmentation and tracking. For instance, a cyclic temporal model was used for periodic cardiac motion [12], [13]. However, due to the substantial variability in the dynamics of the LV of a normal heart, accurate representation of the motion with a single Markovian model is not sufficient. Moreover, dynamics of an abnormal heart could be very different from that of a normal heart. Therefore, the LV dynamics can be viewed as a *Markovian switching system*, which has both *continuous* (noise) and *discrete* (model) uncertainties. For such switching systems, the interacting multiple model (IMM) [14]–[16] is an effective solution. Furthermore, the IMM yields the model probability indicating the model that most closely matches the LV motion at each time step.

In IMM filtering, the state estimates at current time step are updated using only the past observations. However, in cardiac MRI, the data is available upfront. As such, IMM *fixed-interval* smoothing [17] can be further exploited for our problem.

The proposed method is evaluated quantitatively by comparison with independent manual segmentations over 2280 images

Manuscript received July 16, 2009; revised October 7, 2009, January 26, 2010, and March 2, 2010; accepted March 17, 2010. Date of publication May 24, 2010; date of current version July 14, 2010. The work of K. Punithakumar was supported in part by the Natural Sciences and Engineering Research Council of Canada, under the Industrial Research and Development Fellowship. *Asterisk indicates corresponding author.*

*K. Punithakumar is with the GE Healthcare, London, ON N6A 4V2, Canada (e-mail: kumaradevan.punithakumar@ge.com).

I. Ben Ayed is with the GE Healthcare, London, ON N6A 4V2, Canada.

A. Islam is with the St. Joseph's Health Care, London, ON N6A 5B8, Canada.

I. G. Ross is with the London Health Science Center, London, ON N6A 5W9 Canada.

S. Li is with the GE Healthcare, London, ON N6A 4V2, Canada, and also with the University of Western Ontario, London, ON N6G 1G9, Canada.

Color versions of one or more of the figures in this paper are available online at http://ieeexplore.ieee.org.

Digital Object Identifier 10.1109/TBME.2010.2048752

[1]Typically, the number of images per subject is equal to 200.

acquired from 20 subjects, which demonstrated competitive results in comparisons with recent methods: level set overlap prior (LSOP) [1] and GCDM [11].

The remainder of this paper is organized as follows. Section II describes the LV cavity segmentation using the GCDM method. In Section III, we introduce a general model to characterize the dynamics of LV cavity points. The proposed multiple model approach is described in Section V. Experimental evaluations over 2280 images as well as comparison of the proposed method with other recent methods are described in Section VI. Finally, conclusions are given in Section VII.

II. Graph Cut Distribution Matching

Let $\mathbf{I}_p^n = \mathbf{I}^n(p) : \mathcal{P} \subset \mathbb{R}^2 \rightarrow \mathcal{I}, n \in [1, \ldots, N]$, be a MR cardiac sequence, with N is the number of frames in the sequence,[2] $\mathcal{P}$ is the positional array, and $\mathcal{I}$ is the space of photometric variables.

The first stage consists of finding for each frame $n \in [2, \ldots, N]$, a partition of $\mathcal{P}$ into two regions: the *heart cavity* and its complement in $\mathcal{P}$. We use the GCDM in [11], which yields initial segmentation of the LV cavity within each frame by keeping the same photometric/geometric distribution of the cavity over cardiac cycles. This is done by minimizing a discrete cost function with respect to a binary variable (labeling) $\mathcal{L}^n(p) : \mathcal{P} \rightarrow \{0, 1\}$, which defines a variable partition of $\mathcal{P}$: the *heart cavity* $\mathbf{C}^n$ corresponding to region $\{p \in \mathcal{P}/\mathcal{L}^n(p) = 1\}$ and its complement, the *background* $\mathbf{B}^n$ corresponding to region $\{p \in \mathcal{P}/\mathcal{L}^n(p) = 0\}$. The cost function contains two kernel density matching terms: an intensity matching and a distance matching term. To introduce these terms, we consider the following definitions for any labeling $\mathcal{L} : \mathcal{P} \rightarrow \{0, 1\}$, any image $\mathbf{I} : \mathcal{P} \subset \mathbb{R}^2 \rightarrow \mathcal{I}$, and any space of variables $\mathcal{I}$.

1) $\mathbf{P}^{\mathcal{I}}_{\mathcal{L},\mathbf{I}}$ is the kernel density estimate (KDE) of the distribution of image data $\mathbf{I}$ within region $\mathbf{R}_{\mathcal{L}} = \{p \in \mathcal{P}/\mathcal{L}(p) = 1\}$

$$\forall i \in \mathcal{I}, \quad \mathbf{P}^{\mathcal{I}}_{\mathcal{L},\mathbf{I}}(i) = \frac{\sum_{p \in \mathbf{R}_{\mathcal{L}}} K(i - \mathbf{I}_p)}{\mathbf{A}_{\mathcal{L}}} \tag{1}$$

with

$$K(y) = \frac{1}{\sqrt{2\pi\sigma^2}} \exp(-y^2/2\sigma^2) \tag{2}$$

and $\mathbf{A}_{\mathcal{L}}$ is the number of pixels within $\mathbf{R}_{\mathcal{L}}$

$$\mathbf{A}_{\mathcal{L}} = \sum_{\mathbf{R}_{\mathcal{L}}} 1. \tag{3}$$

σ is the width of the Gaussian kernel.

2) $\mathcal{B}(f, g)$ is the *Bhattacharyya* coefficient[3] measuring the amount of overlap (similarity) between two distributions f and g

$$\mathcal{B}(f, g) = \sum_{i \in \mathcal{I}} \sqrt{f(i)g(i)}. \tag{4}$$

[2]The number of frames N is typically equal to 20 or 25.

[3]Note that the values of $\mathcal{B}$ are always in $[0, 1]$, where 0 indicates that there is no overlap, and 1 indicates a perfect match between the distributions.

We assume that a segmentation of frame $\mathbf{I}^1$ is given. Using this prior information, i.e., a labeling $\mathcal{L}^1$ defining a partition $\{\mathbf{C}^1, \mathbf{B}^1\}$, we learn the photometric and geometric model distributions of the cavity, and optimize the following distribution matching constraints to segment subsequent frames.

A. Photometric Constraint

Given the learned model of intensity, which we denote $\mathbf{M}^{\mathcal{I}} = \mathbf{P}^{\mathcal{I}}_{\mathcal{L}^1,\mathbf{I}^1}$, our purpose is to find for each subsequent frame $\mathbf{I}^n$ a region $\mathbf{C}^n$, whose intensity distribution most closely matches $\mathbf{M}^{\mathcal{I}}$. This can be achieved by minimizing the following intensity matching function with respect to $\mathcal{L}$:

$$\mathcal{B}^{\mathcal{I}}(\mathcal{L}, \mathbf{I}^n) = -\mathcal{B}(\mathbf{P}^{\mathcal{I}}_{\mathcal{L},\mathbf{I}^n}, \mathbf{M}^{\mathcal{I}}) = -\sum_{i \in \mathcal{I}} \sqrt{\mathbf{P}^{\mathcal{I}}_{\mathcal{L},\mathbf{I}^n}(i)\mathbf{M}^{\mathcal{I}}(i)}. \tag{5}$$

B. Geometric Constraint

The purpose of this term is to constrain the segmentation with prior geometric information (shape, scale, and position of the cavity) obtained from the learning frame. Let c be the centroid of cavity $\mathbf{C}^1$ in the learning frame and $\mathbf{D}(p) = \|p - c\|/N_{\mathbf{D}} : \mathcal{P} \rightarrow \mathcal{D}$ *be a distance image* measuring the normalized distance between p and c, with D the space of distance variables and $N_{\mathbf{D}}$ a normalization constant. Let $\mathbf{M}^{\mathcal{D}} = \mathbf{P}^{\mathcal{D}}_{\mathcal{L}^1,\mathbf{D}}$ be the model distribution of distances within the cavity in the learning frame. We seek a region $\mathbf{C}^n$, whose distance distribution most closely matches $\mathbf{M}^{\mathcal{D}}$ by minimizing

$$\mathcal{B}^{\mathcal{D}}(\mathcal{L}, \mathbf{D}) = -\mathcal{B}(\mathbf{P}^{\mathcal{D}}_{\mathcal{L},\mathbf{D}}, \mathbf{M}^{\mathcal{D}}) = -\sum_{d \in \mathcal{D}} \sqrt{\mathbf{P}^{\mathcal{D}}_{\mathcal{L},\mathbf{D}}(d)\mathbf{M}^{\mathcal{D}}(d)}. \tag{6}$$

C. Segmentation Cost Function

The cost function contains the photometric and geometric matching terms as well as a smoothness term. For each $n \in [2, \ldots, N]$, the first stage of our algorithm computes the optimal labeling $\mathcal{L}^n_{\text{opt}}$ minimizing

$$\mathcal{F}(\mathcal{L}, \mathbf{I}^n) = \mathcal{B}^{\mathcal{I}}(\mathcal{L}, \mathbf{I}^n) + \mathcal{B}^{\mathcal{D}}(\mathcal{L}, \mathbf{D}) + \lambda \mathbf{S}(\mathcal{L}) \tag{7}$$

where $\mathbf{S}(\mathcal{L})$ is related to the length of the partition boundary given by [18]

$$\mathbf{S}(\mathcal{L}) = \sum_{\{p,q\} \in \mathcal{N}} \frac{\delta_{\mathcal{L}_p \neq \mathcal{L}_q}}{\|p - q\|}, \text{ with } \delta_{x \neq y} = \begin{cases} 1, \text{ if } x \neq y \\ 0, \text{ if } x = y \end{cases} \tag{8}$$

and $\mathcal{N}$ is a neighborhood system containing all unordered pairs $\{p, q\}$ of neighboring elements of $\mathcal{P}$. λ is a positive constant that balances the relative contribution of $\mathbf{S}$.

D. Optimization

Optimization of the distribution matching terms in $\mathcal{F}(\mathcal{L}, \mathbf{I}^n)$ is non-deterministic polynomial-time (*NP*)-*hard*, and does not afford an analytical form amenable to graph cut optimization. To compute initial segmentations efficiently, we use the method in [11]. Rather than minimizing directly the cost function, Ben

Ayed *et al.* [11] proposed a first-order approximation of the Bhattacharyya measure, which allows to optimize $\mathcal{F}(\mathcal{L}, \mathbf{I}^n)$ with a fast graph cut computation [19]. Alternatively, one can use a gradient-descent level set optimization as in [1], but this leads to a computationally intensive algorithm.

This first stage based on the method[4] in [11], computes only independent frame segmentations, and therefore, does not constrain the LV tracking with temporal consistency. In the next sections (see Sections III and V), we propose a multiple model filtering approach, which allows to characterize the dynamic behavior of the LV. This approach yields LV motion estimation, and as we will show experimentally (see Section VI), enhances the segmentation results in comparisons to the methods in [1] and [11].

III. Dynamic Model for Temporal Periodicity

For any frame, let $\mathcal{L}^n_{\text{opt}}$ be the optimal labeling obtained with GCDM, and let (x, y) be a Cartesian point sampled on the boundary between the segmentation regions defined by $\mathcal{L}^n_{\text{opt}}$, i.e., the set of points, where the gradient of $\mathcal{L}^n_{\text{opt}}$ is not equal to zero. Consider the state vector $\xi = [\bar{\mathsf{x}}\ \mathsf{x}\ \dot{\mathsf{x}}]^T$ that describes the dynamics of the point in x-coordinate direction, where $\dot{\mathsf{x}}$ and $\bar{\mathsf{x}}$ denote velocity and the mean position over cardiac cycle, respectively. We assume the heart motion is periodic. Then, we can define a *continuous state-space* model that describes the cyclic motion of the point as follows:

$$\dot{\xi}(t) = A(\omega)\xi(t) + B\mathsf{w}(t) \tag{9}$$

where $A(\omega) = \begin{bmatrix} 0 & 0 & 0 \\ 0 & 0 & 1 \\ \omega^2 & -\omega^2 & 0 \end{bmatrix}$, $B = \begin{bmatrix} 1 & 0 \\ 0 & 0 \\ 0 & 1 \end{bmatrix}$, ω is the angular frequency, and $\mathsf{w}(t)$ is the vector-valued white noise that accounts for approximating the unpredictable modeling errors arising in LV motion. Model (9) is linear for a given ω and can be viewed as an approximation of the temporal periodic model used in [13], where the higher order terms of the Fourier expansion were neglected. A bank of models can be effectively used in parallel to closely match the changing dynamics of boundary points, as discussed in Section V. We derive the *discrete-time equivalent*[5] of (9) as follows (refer to Appendix A for derivation details):

$$\xi_{k+1} = F(\omega)\xi_k + \mathsf{w}_k \tag{10}$$

where

$$F(\omega) = \begin{bmatrix} 1 & 0 & 0 \\ 1-\cos(\omega T) & \cos(\omega T) & \frac{1}{\omega}\sin(\omega T) \\ \omega\sin(\omega T) & -\omega\sin(\omega T) & \cos(\omega T) \end{bmatrix}$$

w_k is a discrete-time white noise sequence and T is the sampling interval. The covariance of process noise $Q_k = \text{cov}(\mathsf{w}_k)$ is given by

$$Q_k = [q_{ij}]_{3\times 3} \tag{11}$$

where q_{ij}'s are defined in (64)–(69) in Appendix A. We extend the dynamic model to x–y plane by defining the state vector $\mathbf{s} = [\bar{\mathsf{x}}\ \mathsf{x}\ \dot{\mathsf{x}}\ \bar{\mathsf{y}}\ \mathsf{y}\ \dot{\mathsf{y}}]^T$. The discrete state-space model in x–y plane is given as follows:

$$\mathbf{s}_{k+1} = \begin{bmatrix} F(\omega) & \mathbf{0}_{3\times 3} \\ \mathbf{0}_{3\times 3} & F(\omega) \end{bmatrix} \mathbf{s}_k + v_k = F_k\mathbf{s}_k + v_k. \tag{12}$$

Using a single Markovian model as in (12) is insufficient to describe the LV dynamics due to the following reasons: 1) the angular frequency that characterizes the motion of a LV point for normal subjects changes over time; 2) the dynamics of LV motion differ significantly in systolic and diastolic phases of heart beat; and 3) the LV dynamics of abnormal subjects differ significantly from those of normal subjects.

Therefore, the LV dynamics is a *hybrid system*—a system which has both *continuous* (noise) and *discrete* (model) uncertainties.

IV. Background on Multiple Model Filtering

Our objective is to build a Bayesian estimation of the dynamics of the LV given multiple models rather than a single model. The direct approach to the problem is a choice as to the model to be used followed by estimation, i.e., it first chooses the best model based on which it runs a single model filter. However, in this approach, possible errors in the choice of the model are not accounted for in the estimation. Further, the approach cannot take advantage of the estimation results in model choice.

More willingly, multiple model approaches by detecting the maneuvers, i.e., switching between different modes, and identifying the appropriate model have been shown very effective. Each model is designed to represent a certain mode or dynamic behavior of the system, the dynamics of the LV in our case. Starting with prior probabilities for each model, a Bayesian framework is used to calculate the posterior model probabilities. Here, we assume the system undergoes transition from one mode to another. Thus, the optimal solution is intractable in practice, since each possible mode sequence requires a filter, which results in an exponentially increasing number of filters, i.e., the optimal filtering with n models requires n^k filters for processing kth observation to estimate state $\mathbf{s}_k$.

Alternatively, suboptimal approaches combine only the past estimates with the highest probabilities and discard the rest. For example, in the case of generalized pseudo-Bayesian (GPB) filters [16], the first-order filter GPB_1, considers only the possible models in the last sampling period, whereas the second-order filter GPB_2, considers all the possible models in the last two sampling periods. These algorithms require n and n^2 filters to operate in parallel, respectively. Another well-known suboptimal approach to hybrid estimation problem is the IMM filter [16]. It is conceptually similar to GPB_2, but requires only n filters to operate in parallel. This is achieved by mixing the hypotheses at the beginning of each filtering cycle. Thus, the performance of the IMM algorithm closely approximates that

[4]Note that one can use a different segmentation method as a first stage, for instance, the method in [1]. However, in this paper, we use the graph cut optimization in [11] because it leads to a fast algorithm.

[5]The term discrete-time equivalent refers to the model if the discretization is exact and the continuous and discrete-time process noises have equivalent effects.

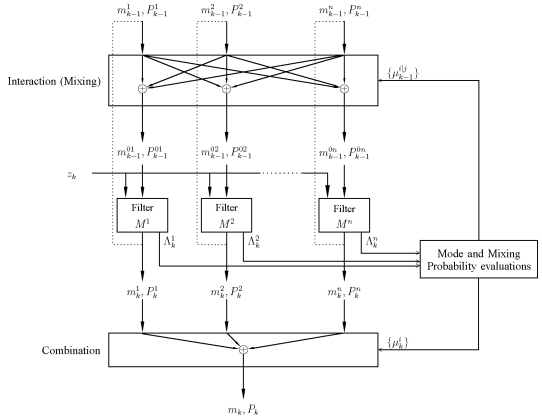

Fig. 1. IMM estimator (forward time).

of the GPB_2, while requiring computational resource slightly more than that of GPB_1. The final estimate in IMM filtering is a weighted sum of each individual filters, and thus, enables a *soft decision*.

V. IMM Filter

Let

$$M = \{M^1, \ldots, M^n\}$$

be the system, which consists of a discrete set of n models. In the IMM filter, the state estimate at any time is computed under each model with n filters, each using a different combination of the previous model-conditioned estimates (cf., Fig. 1 for an illustration). Let $\mu_1^j = P\{M_1^j\}$ be the prior probability of model M^j at time step 1 (the initial time step). In our example, we consider a semi-Markov process, i.e., from any model M^i, the next to take place M^j, is chosen at random according to an assumed model transition probability p_{ij}. The system of equations corresponding to M_k^j is given by

$$\mathbf{s}_k = F_k^j \mathbf{s}_{k-1} + v_{k-1}^j \tag{13}$$

$$z_k = H_k \mathbf{s}_k + \eta_k^j \tag{14}$$

where η_k^j is zero-mean Gaussian noise sequence with covariance R_k^j and

$$H_k = \begin{bmatrix} B_k & \mathbf{0}_{1\times 3} \\ \mathbf{0}_{1\times 3} & B_k \end{bmatrix} \tag{15}$$

$$B_k = \begin{bmatrix} 0 & 1 & 0 \end{bmatrix}. \tag{16}$$

Each cycle of the IMM filter is composed of interaction, model specific filtering, model probability update, and combination steps. Calculation of initial mean $\{m_1^j\}$ and covariance $\{P_1^j\}$ inputs to the IMM is given in Section V-B.

Interaction: The individual filter estimates are mixed with respect to the predicted model probabilities. The mixing probabilities $\mu_k^{i|j}$ for models M^i and M^j are calculated as follows:

$$\mu_k^{i|j} = \frac{1}{\bar{c}_j} \sum_{i=1}^{n} p_{ij} \mu_{k-1}^i \tag{17}$$

with $\bar{c}_j$ is given by

$$\bar{c}_j = \sum_{i=1}^{n} p_{ij} \mu_{k-1}^i \tag{18}$$

and μ_{k-1}^i is the model probability at time step $k-1$. The inputs (mean and covariance) to each filter j are calculated by

$$m_{k-1}^{0j} = \sum_{i=1}^{n} \mu_k^{i|j} m_{k-1}^i$$

$$P_{k-1}^{0j} = \sum_{i=1}^{n} \mu_k^{i|j} \left[P_{k-1}^i + (m_{k-1}^i - m_{k-1}^{0j})(m_{k-1}^i - m_{k-1}^{0j})^T \right].$$

Model specific filtering: Each filter predicts and updates its state estimate using its dynamic model assumption. The Kalman filter [16] is used to calculate the mode-conditioned state estimates for each model. The prediction and update equations are given by

$$[m_k^{-,i},\ P_k^{-,i}] = \text{KF}_p(m_{k-1}^{0j}, P_{k-1}^{0j}, F(\omega^i), Q_k^i)$$

$$[m_k^i,\ P_k^i] = \text{KF}_u(m_k^{-,i}, P_k^{-,i}, z_k, H_k^i, R_k^i)$$

where KF_p and KF_u denote prediction and update equations of Kalman filter, respectively.

Model probability update: The probability of a model being correct (mode probability) is updated with respect to its measurement residual, the difference between the actual and predicted measurements. The mode probability μ_k^i of model M_k^j is computed as follows:

$$\mu_k^i = \frac{\Lambda_k^i \bar{c}_i}{\sum_{i=1}^{n} \Lambda_k^i \bar{c}_i} \tag{19}$$

where Λ_k^i denotes the likelihood of model M^i at time step k, given by

$$\Lambda_k^i = \mathcal{N}(v_k^i; 0, S_k^i) \tag{20}$$

with v_k^i is the measurement residual and S_k^i is innovation covariance for model M^i in the Kalman filter update step.

Combination: The estimate of the IMM algorithm is calculated by combining individual mode-conditioned filter estimates using mode probabilities as follows:

$$m_k = \sum_{i=1}^{n} \mu_k^i m_k^i$$

$$P_k = \sum_{i=1}^{n} \mu_k^i \left[P_k^i + (m_k^i - m_k)(m_k^i - m_k)^T \right].$$

A. Fixed-Interval IMM Smoother

To estimate state $\mathbf{s}_k$, the IMM filter uses only the set observations $z_{1:k}$ from time step 1 to k. However, since the data in

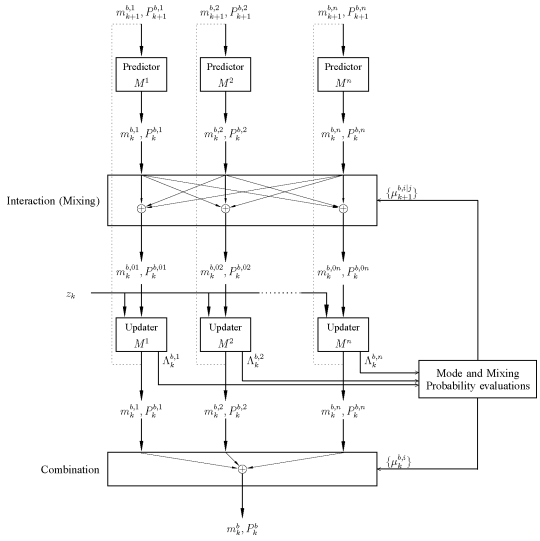

Fig. 2. Backward-time IMM filter.

cardiac MRI is available upfront, the performance of the filtering algorithm can be improved drastically by smoothing [17], [20], [21] the estimation of state $\mathbf{s}_k$ using observations $z_{k:N}$, where $N > k$. There are several variants of smoothing [22], the most common being *fixed-interval smoothing*, which we use here. The optimal solution for fixed-interval smoothing is to fuse the posterior distributions obtained by two optimal IMM estimators, one running forward and the other backward using an equivalent reverse-time Markov model. However, obtaining both the equivalent reverse-time model and optimal forward/backward-time IMM estimators is difficult. To tackle this problem, the approximate fixed-interval smoother [17] uses an approximate backward-time filter that generates the maximum-likelihood estimate of the state given the future observations, but does not use any of the prior statistics of the state. These maximum-likelihood estimates can be viewed as Bayesian estimates under the assumption that the state in the backward-time filter can be described as diffuse prior density [16]. This avoids constructing a reversed-Markov model.

1) Backward-Time IMM Filter: The block diagram of backward-time IMM filtering is presented in Fig. 2. Using total probability theory, the backward-time filtering density $P(\mathbf{s}_k|z_{k:N})$ can be expressed as follows:

$$P(\mathbf{s}_k|z_{k:N}) = \sum_{j=1}^{n} \mu_k^{b,j} p(\mathbf{s}_k^j|z_{k:N}) \tag{21}$$

where $\mu_k^{b,j}$ is the model probability of backward-time filter M_k^j at time step k. The backward-time filter is initialized at the last time step N, and the forward and backward-time filters' model probabilities at N will be the same, i.e., $\mu_N^{b,j} = \mu_N^j$. The model-conditioned backward-time filtering densities can be expressed as follows:

$$p(\mathbf{s}_k^j|z_{k:N}) = \frac{1}{c} p(z_{k:N}|\mathbf{s}_k^j) p(\mathbf{s}_k^j|z_{k+1:N}) \tag{22}$$

where c is a normalizing constant. The model-conditioned density $p(\mathbf{s}_k^j|z_{k+1:N})$ given the future measurements $z_{k+1:N}$ is expressed as follows:

$$p(\mathbf{s}_k^j|z_{k+1:N}) = \sum_{j=1}^{n} \mu_{k+1}^{b,i|j} p(\mathbf{s}_k^j|M_{k+1}^j, z_{k+1:N}) \tag{23}$$

where the conditional mode probability $\mu_{k+1}^{b,i|j}$ is computed as follows:

$$\mu_{k+1}^{b,i|j} = P\{M_{k+1}^i|M_k^j, z_{k+1:N}\} = \frac{1}{a_j} p_{ij}^{b,k} \mu_{k+1}^{b,i}. \tag{24}$$

The normalization constant a_j is given by

$$a_j = \sum p_{ij}^{b,k} \mu_{k+1}^{b,i}. \tag{25}$$

The density $p(\mathbf{s}_k^j|M_{k+1}^j, z_{k+1:N})$ is approximated with a Gaussian $\mathcal{N}(\mathbf{s}_k|\hat{m}_k^{b,i},\ \hat{P}_k^{b,i})$. The mean and covariance of one-step backward-time filter estimate are given by the Kalman filter prediction using the inverse of the state transition matrix as follows:

$$[\hat{m}_k^{b,i},\ \hat{P}_k^{b,i}] = \mathrm{KF}_p(m_{k+1}^{b,i}, P_{k+1}^{b,i}, F(\omega^i)^{-1}, Q_k^i). \tag{26}$$

The density $p(\mathbf{s}_k^j|z_{k+1:N})$ can be approximated by a Gaussian density with mean $\hat{m}_k^{b,0j}$ and covariance $\hat{P}_k^{b,0j}$, where

$$\hat{m}_k^{b,0j} = \sum_{i=1}^{n} \mu_{k+1}^{b,i|j}, m_k^{b,i}$$

$$P_k^{b,0j} = \sum_{i=1}^{n} \mu_{k+1}^{b,i|j} \left[\hat{P}_k^{b,i} + (\hat{m}_k^{m,i} - \hat{m}_k^{b,0j})(\hat{m}_k^{m,i} - \hat{m}_k^{b,0j})^T\right].$$

The aforementioned mixing procedure is slightly different from that of IMM filter, where the filtered estimate from the previous stage are mixed before using a forward-time one-step predictor. This difference is due to the fact that M_k^j is associated with the sampling period $(t_{k-1}, t_k]$, and in the backward-time filter, the previous filtered estimates are valid at t_{k+1}. Therefore, these previous estimates cannot be mixed at t_{k+1} and must first be predicted back to t_k using M_{k+1}^j, which is in effect over $(t_k, t_{k+1}]$. These estimates can then be mixed conditioned on M_k^j. We refer to [17] for further details.

The mean $m_k^{b,j}$ and covariance $P_k^{b,j}$ of the updated backward-time filter density $p(\mathbf{s}_k^j|z_{k:N})$ is computed by the Kalman filter update as follows:

$$[m_k^{b,j},\ P_k^{b,j}] = \mathrm{KF}_u(\hat{m}_k^{b,0j}, \hat{P}_k^{b,0j}, z_k, H_k^j, R_k^j). \tag{27}$$

The measurement likelihoods for each model are computed as follows:

$$\Lambda_k^{b,i} = \mathcal{N}(v_k^{b,i}; 0, S_k^{b,i}) \tag{28}$$

where $v_k^{b,i}$ is the measurement residual and $S_k^{b,i}$ is the innovation covariance for model M^i in the Kalman filter update step. We now can update the model probabilities $\mu_k^{b,j}$ at time step k

$$\mu_k^{b,j} = \frac{1}{a} a_j \Lambda_k^{b,j} \tag{29}$$

where the normalizing constant a is given by

$$a = \sum_{j=1}^{m} a_j \Lambda_k^{b,j}. \tag{30}$$

The mean m_k^b and covariance P_k^b of the Gaussian approximation of the updated density $p(\mathbf{s}_k|z_{k:N})$ is given by

$$m_k^b = \sum_{j=1}^{n} \mu_k^{b,j} m_k^{b,j}$$

$$P_k^b = \sum_{j=1}^{n} \mu_k^{b,j} \left[P_k^{b,j} + (m_k^{b,j} - m_k^b)(m_k^{b,j} - m_k^b)^T \right].$$

2) Two Filter-Based Fixed-Interval IMM Smoother: This section describes the suboptimal fixed-interval smoothing algorithm for Markovian switching systems that fuses the estimates from forward and backward-time IMM filters. The objective of the smoothing process is to find an estimate for $\mathbf{s}_k$ at time-step k using measurements from 1 to N, where $N > k$. The smoothing density can be expressed as follows:

$$p(\mathbf{s}_k|z_{1:N}) = \sum_{j=1}^{n} \mu_k^{s,j} p(\mathbf{s}_k^j|z_{1:N}) \tag{31}$$

where the model probabilities are computed as follows:

$$\mu_k^{s,j} = P\{M_k^j|z_{1:N}\} = \frac{d_j \mu_k^k}{\sum_{j=1}^{n} d_j \mu_k^k} \tag{32}$$

and

$$d_j = p(z_{k+1:N}|M_k^j, z_{1:k}) \tag{33}$$

will be evaluated later in (36). The model-conditioned smoothing distributions $p(\mathbf{s}_k^j|z_{1:N})$ are expressed as mixture of Gaussian distributions as follows:

$$p(\mathbf{s}_k^j|z_{1:N}) = \sum_{j=1}^{n} \mu_{k+1}^{s,i|j} p(\mathbf{s}^i|M_{k+1}^j, z_{1:N}) \tag{34}$$

where the conditional probability is given by

$$\mu_{k+1}^{s,i|j} = P\{M_{k+1}^i|M_k^j, z_{1:N}\} = \frac{1}{d_j} p_{ij} \Lambda_k^{ij} \tag{35}$$

and the likelihood Λ_k^{ij} by

$$\Lambda_k^{ij} = p(z_{k+1:N}|M_k^j, M_{k+1}^i, z_{1:k}) \approx p(\hat{\mathbf{s}}_k^{b,i}|M_k^j, M_{k+1}^i, \mathbf{s}_k^j).$$

This means that future measurements $z_{k+1:N}$ are replaced with n model-conditioned backward-time predicted means and covariances $\{\hat{m}_k^{b,i}, \hat{P}_k^{b,i}\}$, and $z_{1:k}$ will be replaced by n model-conditioned forward-time filtered means and covariances $\{\hat{m}_k^i, \hat{P}_k^i\}$. Then, the likelihoods can be evaluated as follows:

$$\Lambda_k^{ij} = \mathcal{N}(\hat{m}_k^{b,i} - m_k^j|0, \hat{P}_k^{b,i} + P_k^j).$$

Terms d_j can be computed as follows:

$$d_j = \sum_{i=1}^{n} p_{ji} \Lambda_k^{ij}. \tag{36}$$

The smoothing distribution of the states matched to M_k^j and M_{k+1}^i over two successive sampling periods can be expressed as follows:

$$p(\mathbf{s}_k^j|M_{k+1}^i, z_{1:N}) = \frac{1}{c} p(z_{k+1:N}|M_{k+1}^i, \mathbf{s}_k) p(\mathbf{s}_k^j|z_{1:k}) \tag{37}$$

where $p(z_{k+1:N}|M_{k+1}^i, \mathbf{s}_k)$ is the forward-time model-conditioned distribution, $p(\mathbf{s}_k^j|z_{1:k})$ is the backward-time one-step predictive distribution, and c is a normalizing constant. Thus, the smoothing distribution can be expressed as follows:

$$p(\mathbf{s}_k^j|M_{k+1}^i, z_{1:N}) \propto \mathcal{N}(\mathbf{s}_k|\hat{m}_k^{b,i}, \hat{P}_k^{b,i}) \mathcal{N}(\mathbf{s}_k|m_k^i, P_k^i)$$
$$= \mathcal{N}(\mathbf{s}_k|m_k^{s,ji}, P_k^{s,ji})$$

where

$$m_k^{s,ji} = P_k^{s,ji} \left[(P_k^i)^{-1} m_k^i + (\hat{P}_k^{b,i})^{-1} \hat{m}_k^{b,i} \right]$$

$$P_k^{s,ji} = \left[(P_k^i)^{-1} + (\hat{P}_k^{b,i})^{-1} \right]^{-1}.$$

The model-conditioned smoothing distributions are approximated by a Gaussian with mean $m_k^{s,j}$ and covariance $P_k^{s,j}$ as follows:

$$m_k^{s,j} = \sum_{i=1}^{n} \mu_{k+1}^{s,i|j} m_k^{s,ji}$$

$$P_k^{s,j} = \sum_{i=1}^{n} \mu_{k+1}^{s,i|j} \left[P_k^{s,ji} + (m_k^{s,ji} - m_k^{s,j})(m_k^{s,ji} - m_k^{s,j})^T \right].$$

Finally, similar to forward/backward-time IMM filters, we can match the moments of the overall smoothing distribution to approximate it as a Gaussian with mean m_k^s and covariance P_k^s

$$m_k^s = \sum_{j=1}^{n} \mu_k^{s,j} m_k^{s,ji}$$

$$P_k^s = \sum_{j=1}^{n} \mu_k^{s,j} \left[P_k^{s,j} + (m_k^{s,j} - m_k^s)(m_k^{s,j} - m_k^s)^T \right].$$

B. Filter Initialization

In our problem, we do not have *prior* knowledge of the initial value of $\mathbf{s}_1$. Therefore, we use *two-point differencing* method [16] to initialize position and velocity components of the state. For instance, the initial position and velocity elements in x-coordinate direction are given by

$$\hat{\mathrm{x}}_1 = z_{1,\mathrm{x}} \tag{38}$$

$$\hat{\dot{\mathrm{x}}}_1 = \frac{(z_{2,\mathrm{x}} - z_{1,\mathrm{x}})}{T}. \tag{39}$$

The mean position over cardiac cycle $\bar{\mathrm{x}}$ is initialized by taking the expectation over all corresponding measurements

$$\hat{\bar{\mathrm{x}}}_1 = \frac{1}{K} \sum_{k=1}^{K} z_{k,\mathrm{x}}. \tag{40}$$

The initial state elements in y-coordinate direction $\hat{\mathrm{y}}_1$, $\hat{\dot{\mathrm{y}}}_1$, and $\hat{\bar{\mathrm{y}}}_1$, can be computed similarly using $\{z_{k,\mathrm{y}}\}$ and the initial mean

input $m_1^j = [\hat{x}_1\ \hat{\dot{x}}_1\ \hat{\ddot{x}}_1\ \hat{y}_1\ \hat{\dot{y}}_1\ \hat{\ddot{y}}_1]^T$. The corresponding covariance is given by

$$P_1^j = \begin{bmatrix} \Phi_1 & \mathbf{0}_{3\times 3} \\ \mathbf{0}_{3\times 3} & \Phi_1 \end{bmatrix} \tag{41}$$

where

$$\Phi_1 = \begin{bmatrix} r & \frac{r}{K} & \frac{r}{KT} \\ \frac{r}{K} & r & \frac{r}{T} \\ \frac{r}{KT} & \frac{r}{T} & \frac{2r}{T^2} \end{bmatrix}. \tag{42}$$

VI. Experiments

The proposed method was applied to 120 short-axis sequences of cardiac cine MR images, with a temporal resolution of 20 frames/cardiac cycle, acquired from 20 subjects. The images were acquired on 1.5T MRI scanners with fast-imaging employing steady-state acquisition (FIESTA) image sequence mode. The endocardial boundary was tracked in a total of 2280 images, including apical, mid-cavity, and basal slices, and the results were evaluated quantitatively by comparisons with the manual segmentations performed independently by a medical professional. The results were also compared with the recent LV boundary tracking methods, LSOP [1] and GCDM [11], using the same data.

Parameter settings: The regularization and kernel width parameters were unchanged for all the datasets in GCDM: α set equal to 0.15, the kernel width σ to 5 for distance distributions, and to 10 for intensity distributions. Given the high variability in cardiac motion, the dynamic model parameters were chosen so as to characterize both benign and maneuvering motions. Four dynamic models were used in the IMM (the values were measured in squared pixels and $\omega_0 = 2\pi/(\text{heart period})$): 1) $\omega = \omega_0,\ q_1 = 0.02,\ q_2 = 0.1,\ R_k = 1$; 2) $\omega = \omega_0,\ q_1 = 0.2,\ q_2 = 1,\ R_k = 1$; 3) $\omega = \omega_0,\ q_1 = 2,\ q_2 = 10,\ R_k = 1$; and 4) $\omega = 0.8\omega_0,\ q_1 = 0.2,\ q_2 = 1,\ R_k = 1$.

A. Quantitative Performance Evaluation

We used two criteria to evaluate the performances of the algorithms.

1) Root-Mean-Squared Error: We computed the RMSE by computing the perpendicular distances from manual to automatic LV boundaries using 60 points along the boundary. The RMSE over N number of points is given by

$$\text{RMSE} = \sqrt{\frac{1}{N}\sum_{i=1}^{N}(\hat{x}_i - \tilde{x}_i)^2 + (\hat{y}_i - \tilde{y}_i)^2} \tag{43}$$

where $(\hat{x}_i,\ \hat{y}_i)$ is a point on the automatic boundary and $(\tilde{x}_i,\ \tilde{y}_i)$ is the corresponding point on the manual boundary. Table I reports the RMSE for the proposed method, GCDM and LSOP averaged over all the dataset. The proposed method yielded an RMSE of 2.0 mm, whereas the methods GCDM and LSOP yielded 2.6 and 3.1 mm, respectively. The average RMSE plotted against the time step is shown in Fig. 6(a). The proposed algorithm yielded a lower RMSE compared to other methods, and therefore, a higher conformity to the manual segmentation.

TABLE I
RMSE and DM Statistics for the Proposed Method (GCDM–IMM) and Method in [1]

Performance measure	**RMSE** (mm)	**RMSE** (pixels)	**DM**
GCDM-IMM	2.0	1.5	0.926 ± 0.001
GCDM	2.6	2.0	0.912 ± 0.002
LSOP	3.1	2.4	0.884 ± 0.008

2) Dice Metric: We computed the *dice metric* (DM), a common measure of similarity between manual and automatic segmentation [1], [23]. The DM is given by

$$\text{DM} = \frac{2\mathbf{V_{am}}}{\mathbf{V_a} + \mathbf{V_m}} \tag{44}$$

where $\mathbf{V_a}$, $\mathbf{V_m}$, and $\mathbf{V_{am}}$ are the volumes of the automatically segmented cavity, the corresponding hand-labeled cavity, and the intersection between them, respectively. Note that DM is always between 0 and 1, where 1 means a perfect match. The proposed method yielded a DM equal to 0.926 ± 0.001, whereas the methods GCDM and LSOP yielded 0.912 ± 0.002 and 0.884 ± 0.008, respectively, for all the data analyzed (refer to Table I, where DM is expressed as mean $\pm$ standard deviation). We also evaluated the algorithm using the *reliability function* of the obtained DMs, defined for each $d \in [0, 1]$ as the probability of obtaining DM higher than d over all volumes: $\mathcal{R}(d) = \Pr(\text{DM} > d)$ =(number of volumes segmented with DM higher than d)/(total number of volumes). In comparison to other methods, the proposed algorithm led to a higher reliability curve, as depicted in Fig. 6(b).

B. Visual Inspection

In Figs. 3 and 4, we give a representative sample of the results for three subjects. Fig. 3 shows the trajectory of LV points estimated using the proposed GCDM–IMM method. The first row in Fig. 4 depicts typical examples, where the proposed method included accurately the papillary muscles inside the target cavity, although these have an intensity profile similar to the surrounding myocardium. To demonstrate explicitly, the positive effect of the proposed IMM filtering, we show in Fig. 5, the LV boundary estimated using the GCDM–IMM and GCDM alone, along with the manual segmentation, and reports the corresponding DM values. In these typical examples, the proposed method yielded a significant improvement in accuracy, i.e., a better conformity to manual segmentations, over GCDM.

Our MATLAB implementation of the IMM algorithm running on 2.0 GHz Intel Xeon computer took 2.96 ± 0.02 s to process a sequence of 20 images. The computational time for GCDM is reported in [11].

VII. Discussion

This study investigates the problem of tracking endocardial motion via GCDM and IMM smoothing. GCDM yields

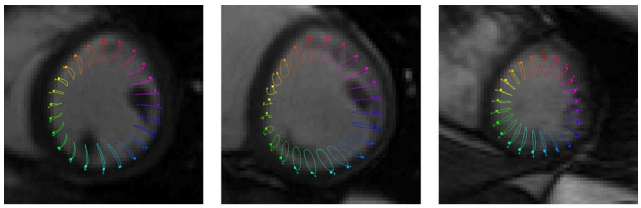

(a) (b) (c)

Fig. 3. Trajectory of LV endocardial boundary points estimated using the proposed method. (a) Mid. (b) Basal. (c) Apical.

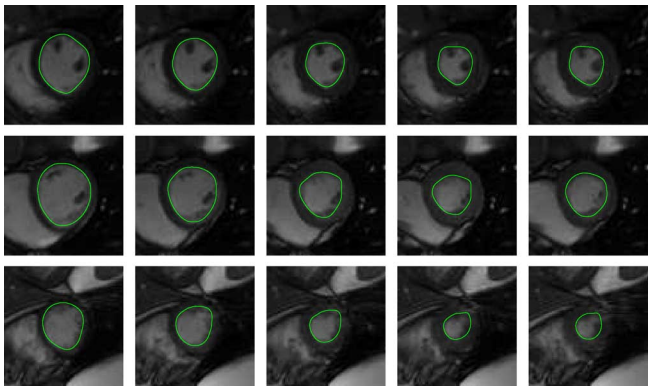

Fig. 4. Representative examples of the LV boundary tracking using the proposed method: mid-cavity (first row), basal (second row), and apical (third row) frames. The first row depicts typical examples, where the proposed method included accurately the papillary muscles inside the target cavity, although these have an intensity profile similar to the surrounding myocardium.

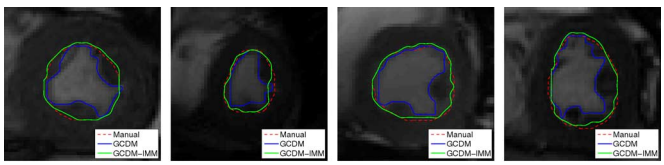

(a) (b) (c) (d)

Fig. 5. Typical examples (with corresponding DM values of estimated boundaries by the GCDM–IMM and GCDM alone), which demonstrate explicitly the positive effect of the proposed IMM filtering. (a) GCDM–IMM $= 0.97$, GCDM $= 0.81$. (b) GCDM–IMM $= 0.96$, GCDM $= 0.78$. (c) GCDM–IMM $= 0.96$, GCDM $= 0.81$. (d) GCDM–IMM $= 0.96$, GCDM $= 0.78$.

initial frame segmentations by keeping the same photometric/geometric distribution of the cavity over cardiac cycles, whereas IMM constrains the results with prior knowledge of temporal consistency. The proposed method is evaluated quantitatively using RMSE and DM, by comparison with independent manual segmentations over 2280 images acquired from 20 subjects, which demonstrated significantly better results as compared to recent methods [1] and [11]. The method is fast; the algorithm needs approximately 3 s to process a sequence, i.e., 20 frames. It is also flexible because it does not require a prior training. It should be noted, however, that this flexibility comes at the price of a reasonable amount of user interaction (a manual segmentation of the first frame) because the proposed method requires a reliable estimates of the distributions of the cavity. Also, the proposed algorithm does not take into account volume consistency, and therefore, an extension of the approach

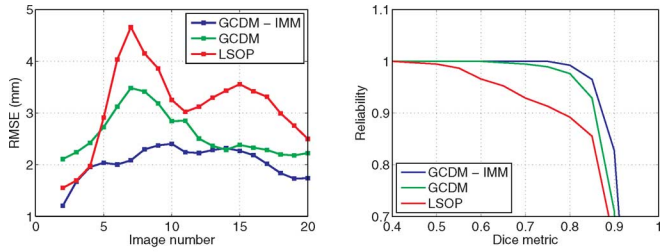

(a) (b)

Fig. 6. Comparison between automatic and manual segmentations of 2280 images acquired from 20 subjects, for the proposed method (GCDM–IMM), GCDM [11] and LSOP [1]. (a) RMSE. (b) Reliability.

to 3-D data is desirable. We are planning to address these issues in our future work.

APPENDIX

DISCRETIZATION OF CONTINUOUS-TIME STATE SPACE MODEL

The continuous-time state equation (9) has the following solution:

$$\xi(t) = F_{cy}(t, t_0)\xi(t_0) + \int_{t_0}^{t} F_{cy}(t, \tau) B \mathsf{w}(\tau) d\tau. \tag{45}$$

The transition matrix has the following properties:

$$\frac{dF_{cy}(t, t_0)}{dt} = A(t) F_{cy}(t, t_0) \tag{46}$$

$$F_{cy}(t_2, t_0) = F_{cy}(t_2, t_1) F_{cy}(t_1, t_0) \qquad \forall t_1 \tag{47}$$

$$F_{cy}(t, t) = I. \tag{48}$$

From (47) and (48), we obtain

$$F_{cy}(t, t_0) = F_{cy}(t, t_0)^{-1}. \tag{49}$$

The transition matrix has no explicit form unless it satisfies the following *commutativity property*:

$$A(t) \int_{t_0}^{t} A(\tau) d\tau = \int_{t_0}^{t} A(\tau) d\tau A(t). \tag{50}$$

Then,

$$F_{cy}(t, t_0) = \exp\left(\int_{t_0}^{t} A(\tau) d\tau \right). \tag{51}$$

For a time-invariant system, assuming $t = 0$

$$F_{cy}(t) \triangleq F_{cy}(t, 0) = \exp(At). \tag{52}$$

The transition matrix A of the continuous state-space model (9) is given by

$$A = \begin{bmatrix} 0 & 0 & 0 \\ 0 & 0 & 1 \\ \omega^2 & -\omega^2 & 0 \end{bmatrix} \tag{53}$$

$$q_{11} = q_1^2 T \tag{64}$$

$$q_{12} = q_{21} = \frac{q_1^2(\omega T - \sin(\omega T))}{\omega} \tag{65}$$

$$q_{13} = q_{31} = q_1^2(1 - \cos(\omega T)) \tag{66}$$

$$q_{22} = \frac{q_1^2\omega^2(3\omega T - 4\sin(\omega T) + \cos(\omega T)\sin(\omega T)) + q_2^2(\omega T - \cos(\omega T)\sin(\omega T))}{2\omega^3} \tag{67}$$

$$q_{23} = q_{32} = \frac{q_1^2\omega^2(1 - 2\cos(\omega T) + \cos^2(\omega T)) + q_2^2\sin^2(\omega T)}{2\omega^2} \tag{68}$$

$$q_{33} = \frac{-q_1^2\omega^2(\cos(\omega T)\sin(\omega T) - \omega T) + q_2^2(\cos(\omega T)\sin(\omega T) - \omega T)}{2\omega} \tag{69}$$

Evaluating $\exp(At)$ yields

$$\exp(At) = \begin{bmatrix} 1 & 0 & 0 \\ 1 - \cos(\omega t) & \cos(\omega t) & \frac{1}{\omega}\sin(\omega t) \\ \omega\sin(\omega t) & -\omega\sin(\omega t) & \cos(\omega t) \end{bmatrix}. \tag{54}$$

The state at sampling time t_{k+1} can be written as follows:

$$\xi(t_{k+1}) = F_{cy}(t_{k+1}, t_k)\xi(t_k) + \mathsf{w}(t_k). \tag{55}$$

For a *time-invariant* continuous-time system, the transition matrix is as follows:

$$\begin{aligned} F_{cy}(t_{k+1}, t_k) &= F_{cy}(t_{k+1} - t_k) \\ &= \exp\left((t_{k+1} - t_k)A\right) \stackrel{\triangle}{=} F_{cy}(k). \end{aligned} \tag{56}$$

The discrete-time process noise relates to that of continuous-time as follows:

$$\mathsf{w}(t_k) = \int_{t_k}^{t_{k+1}} \exp((t_{k+1} - \tau)A)B\mathsf{w}(\tau)d\tau \stackrel{\triangle}{=} \mathsf{w}(k). \tag{57}$$

We assume $\mathsf{w}(t)$ is zero-mean and white noise. It follows that:

$$\mathbb{E}[\mathsf{w}(k)] = \mathbf{0}_{2\times 1} \tag{58}$$

$$\mathbb{E}[\mathsf{w}(k)\mathsf{w}(l)^T] = Q_k\delta_{kl} \tag{59}$$

where δ_{kl} is the Kronecker delta function. The covariance Q_k can be simplified as follows:

$$Q_k = \int_{t_k}^{t_{k+1}} \exp((t_{k+1} - \tau)A)B\Gamma(\tau)B^T \exp((t_{k+1} - \tau)A^T)d\tau \tag{60}$$

where

$$\Gamma(\tau) = \mathbb{E}[\mathsf{w}(\tau)\mathsf{w}(\tau)^T] \tag{61}$$

$$= \begin{bmatrix} q_1^2 & 0 \\ 0 & q_2^2 \end{bmatrix}. \tag{62}$$

Solving (60) yields

$$Q_k = [q_{ij}]_{3\times 3} \tag{63}$$

where (64)–(69) are shown at the top of this page.

REFERENCES

[1] I. Ben Ayed, S. Li, and I. Ross, "Embedding overlap priors in variational left ventricle tracking," *IEEE Trans. Med. Imag.*, vol. 28, no. 12, pp. 1902–1913, Dec. 2009.

[2] A. Pednekar, U. Kurkure, R. Muthupillai, S. Flamm, and I. Kakadiaris, "Automated left ventricular segmentation in cardiac MRI," *IEEE Trans. Biomed. Eng.*, vol. 53, no. 7, pp. 1425–1428, Jul. 2006.

[3] G. Hautvast, S. Lobregt, M. Breeuwer, and F. Gerritsen, "Automatic contour propagation in cine cardiac magnetic resonance images," *IEEE Trans. Med. Imag.*, vol. 25, no. 11, pp. 1472–1482, Nov. 2006.

[4] M.-P. Jolly, H. Xue, L. Grady, and J. Guehring, "Combining registration and minimum surfaces for the segmentation of the left ventricle in cardiac cine MR images," in *Medical Image Computing and Computer-Assisted Intervention 2009* (ser. LNCS 5762), G.-Z. Yang et al., Eds. New York: Springer-Verlag, pp. 910–918.

[5] U. Kurkure, A. Pednekar, R. Muthupillai, S. D. Flamm, and I. A. Kakadiaris, "Localization and segmentation of left ventricle in cardiac cine-MR images," *IEEE Trans. Biomed. Eng.*, vol. 56, no. 5, pp. 1360–1370, May 2009.

[6] H. Lee, N. Codella, M. Cham, J. Weinsaft, and Y. Wang, "Automatic left ventricle segmentation using iterative thresholding and active contour model with adaptation on short-axis cardiac MRI," *IEEE Trans. Biomed. Eng.*, vol. 57, no. 4, pp. 905–913, Apr. 2010.

[7] M. R. Kaus, J. von Berg, J. Weese, W. Niessen, and V. Pekar, "Automated segmentation of the left ventricle in cardiac MRI," *Med. Image Anal.*, vol. 8, no. 3, pp. 245–254, Sep. 2004.

[8] N. Paragios, "A level set approach for shape-driven segmentation and tracking of the left ventricle," *IEEE Trans. Med. Imag.*, vol. 22, no. 6, pp. 773–776, Jun. 2003.

[9] A. Andreopoulos and J. K. Tsotsos, "Efficient and generalizable statistical models of shape and appearance for analysis of cardiac MRI," *Med. Image Anal.*, vol. 12, no. 3, pp. 335–357, Jun. 2008.

[10] M.-P. Jolly, "Automatic recovery of the left ventricular blood pool in cardiac cine MR images," in *Medical Image Computing and Computer-Assisted Intervention 2008* (ser. LNCS 5241), D. Metaxas *et al.*, Eds. New York: Springer-Verlag, pp. 110–118.

[11] I. Ben Ayed, K. Punithakumar, S. Li, A. Islam, and J. Chong, "Left ventricle segmentation via graph cut distribution matching," in *Medical Image Computing and Computer-Assisted Intervention 2009* (ser. LNCS 5762), G.-Z. Yang *et al.* Eds. New York: Springer-Verlag, 2009, pp. 901–909.

[12] B. Spottiswoode, X. Zhong, A. Hess, C. Kramer, E. Meintjes, B. Mayosi, and F. Epstein, "Tracking myocardial motion from cine dense images using spatiotemporal phase unwrapping and temporal fitting," *IEEE Trans. Med. Imag.*, vol. 26, no. 1, pp. 15–30, Jan. 2007.

[13] J. McEachen, A. Nehorai, and J. Duncan, "Multiframe temporal estimation of cardiac nonrigid motion," *IEEE Trans. Image Process.*, vol. 9, no. 4, pp. 651–665, Apr. 2000.

[14] H. Blom and Y. Bar-Shalom, "The interacting multiple model algorithm for systems with Markovian switching coefficients," *IEEE Trans. Autom. Control*, vol. AC-33, no. 8, pp. 780–783, Aug. 1988.

[15] Y. Bar-Shalom, K. Chang, and H. Blom, "Tracking a maneuvering target using input estimation versus the interacting multiple model algorithm," *IEEE Trans. Aerosp. Electron. Syst.*, vol. 25, no. 2, pp. 296–300, Mar. 1989.

[16] Y. Bar-Shalom, T. Kirubarajan, and X.-R. Li, *Estimation with Applications to Tracking and Navigation*. New York, NY: Wiley, 2002.
[17] R. Helmick, W. Blair, and S. Hoffman, "Fixed-interval smoothing for Markovian switching systems," *IEEE Trans. Inf. Theory*, vol. 41, no. 6, pp. 1845–1855, Nov. 1995.
[18] Y. Boykov and V. Kolmogorov, "Computing geodesics and minimal surfaces via graph cuts," in *Proc. IEEE 9th Int. Conf. Comput. Vis.*, Oct., 2003, vol. 1, pp. 26–33.
[19] Y. Boykov and V. Kolmogorov, "An experimental comparison of min-cut/max- flow algorithms for energy minimization in vision," *IEEE Trans. Pattern Anal. Mach. Intell.*, vol. 26, no. 9, pp. 1124–1137, Sep. 2004.
[20] R. Helmick, W. Blair, and S. Hoffman, "One-step fixed-lag smoothers for Markovian switching systems," *IEEE Trans. Autom. Control*, vol. 41, no. 7, pp. 1051–1056, Jul. 1996.
[21] B. Chen and J. Tugnait, "Interacting multiple model fixed-lag smoothing algorithm for Markovian switching systems," *IEEE Trans. Aerosp. Electron. Syst.*, vol. 36, no. 1, pp. 243–250, Jan. 2000.
[22] X. Rong Li and V. Jilkov, "Survey of maneuvering target tracking. Part V: Multiple-model methods," *IEEE Trans. Aerosp. Electron. Syst.*, vol. 41, no. 4, pp. 1255–1321, Oct. 2005.
[23] M. Lynch, O. Ghita, and P. Whelan, "Segmentation of the left ventricle of the heart in 3-D+T MRI data using an optimized nonrigid temporal model," *IEEE Trans. Med. Imag.*, vol. 27, no. 2, pp. 195–203, Feb. 2008.

Kumaradevan Punithakumar received the B.Sc. (Eng.) degree in electronic and telecommunication engineering from the University of Moratuwa, Moratuwa, Sri Lanka, in 2001, and the M.A.Sc. and Ph.D. degrees in electrical and computer engineering from McMaster University, Hamilton, ON, Canada, in 2003 and 2007, respectively.

From 2002 to 2007, he was a Teaching Assistant and, in 2008, a Postdoctoral Research Fellow, both in Electrical and Computer Engineering Department, McMaster University. He is currently an Associate Imaging Research Scientist at GE Healthcare, London, ON, Canada. His research interests include medical image analysis, target tracking, sensor management, and computer vision.

Dr. Punithakumar was the recipient of the Industrial R&D Fellowship by the National Sciences and Engineering Research Council of Canada in 2008.

Ismail Ben Ayed received the Ph.D. degree in computer science from the Institut National de la Recherche Scientifique, Montreal, QC, Canada.

He is currently a Research Scientist with GE Healthcare, London, ON, Canada. His research interests include computer vision, pattern recognition, and medical image analysis.

Ali Islam received the B.Sc. degree from the University of Ottawa, Ottawa, ON, Canada and M.D. degree from the University of Toronto, Toronto, ON, in 1995, and 1999 respectively.

In 2004, he was with the University of Western Ontario, London, ON for residency training in diagnostic radiology. He was a Clinical Fellow in cardiovascular imaging with the Cleveland Clinic, Cleveland, OH, in 2005. He is currently practising and teaching radiology at St. Joseph's Health Care, London, ON and is also the Co-Director of the cardiovascular imaging computed tomography and MRI fellowship at the Schulich School of Medicine, University of Western Ontario. His research interests include segmentation of cardiac images and developing novel collaboration and communications tools for picture archiving and communication system.

Ian G. Ross received the M.D. degree from Queen's University, Kingston, ON, Canada.

He was with Kingston General Hospital, Queen's University for residency training in diagnostic radiology. He was a Clinical Fellow in body musculoskeletal imaging at the University of Western Ontario, London, Ontario for one year. In 2005, he joined as an Assistant Professor of radiology at the University of Western as well as a Staff Radiologist at University Hospital, and since then, he has been performing cross-sectional imaging with a special interest in cardiac computed tomography. He is currently the Medical Leader in General Radiology and Sports Medicine with London Health Science Center, London, ON, where he is actively involved in his research.

Shuo Li received the Ph.D. degree from the Department of Computer Science and Software Engineering, Concordia University, Montreal, QC, Canada, in 2006.

He is currently a Research Scientist and a Project Manager in GE Healthcare, London, ON, Canada. He is also an Adjunct Research Professor in the Department of Medical Biophysics and Medical Imaging, University of Western Ontario, London, ON. He is also the Head of the Digital Imaging Group, London (http://dig.lhsc.on.ca/). His research interests include the computer automated medical image analysis and visualization.